Biosensors and Bioelectronics 24 (2008) 210–215

Contents lists available at ScienceDirect

Biosensors and Bioelectronics

journal homepage: www.elsevier.com/locate/bios

Sensitive label-free biosensors by using gap plasmons in gold nanoslits

Kuang-Li Lee[a,b], Way-Seen Wang[a], Pei-Kuen Wei[b,c,*]

[a] Graduate Institute of Photonics and Optoelectronics, Department of Electrical Engineering, National Taiwan University, No. 1, Section 4, Roosevelt Road, Taipei 10617, Taiwan
[b] Research Center for Applied Sciences, Academia Sinica, No. 128, Section 2, Academic Road, Taipei 11529, Taiwan
[c] National Taiwan Ocean University, Department of Optoelectronics, Keelung, Taiwan

ARTICLE INFO

Article history:
Received 22 January 2008
Received in revised form 20 March 2008
Accepted 25 March 2008
Available online 10 April 2008

Keywords:
Optical biosensors
Nanostructures
Surface plasmon resonance
Cavity mode

ABSTRACT

The detection sensitivities of gap plasmons in gold nanoslit arrays are studied and compared with surface plasmons on outside surface. The nanoslit arrays were fabricated in a 130 nm-thick gold film with various slit widths. For transverse-magnetic (TM) incident wave, the 600 nm-period nanoslit array shows two distinguishable transmission peaks corresponding to the resonances of gap plasmons and surface plasmons, respectively. The surface sensitivities for both modes were compared by coating thin SiO_2 film and different biomolecules on the nanoslit arrays. Our experimental results verify gap plasmons are more sensitive than conventional surface plasmons. Its detection sensitivity increases with the decrease of slit width. The gap plasmon is one order of magnitude sensitive than the surface plasmon for slit widths smaller than 30 nm. We attribute this high sensitivity to the large overlap between biomolecules and nanometer-sized gap plasmons.

1. Introduction

Optical excitation of surface plasmons on a thin metallic surface is widely applied for real-time, label-free, and sensitive biosensing (Knoll, 1998; Silin and Plant, 1997). The conventional method employs attenuated total internal reflection (ATR) in a glass prism to excite surface plasmon resonance (SPR) on a thin gold film coated on the prism. ATR biosensors are known very sensitive to surface environmental changes. The change of surface refractive index can be measured on the order of 10^{-6} by a precise angular measurement (1×10^{-4} degree) or a wavelength shift (0.02 nm) in the optical spectrum (Homola et al., 1999). However, the ATR setup is typically bulky and requires a large amount of sample solution. Due to its optical configuration, it is hard to be applied for high-throughput and chip-based detections, such as DNA microarrays and protein microarrays (Schena et al., 1995; Gavin and Stuart, 2000).

Modern studies of plasmonics in metallic nanostructures have shown that surface plasmons can also be excited by nanoarrays (Ebbesen et al., 1998; Kawata, 2001; Lezec et al., 2002). Surface plasmons are in resonance when their wavelength matches the period of the array. The SPR in the metallic nanoarray results in an extraordinary transmission peak. Similar to the conventional SPR sensor, such nanoarray is expected to have good surface sensitivity. Besides, it has the potential for high-throughput detections. The concept by using an array of nanoholes in gold thin film has been proved by different groups (Brolo et al., 2004; Pang et al., 2007). Recently, chip-based label-free biosensors by using SPR in gold nanoslit arrays were also proposed (Lee et al., 2007).

Different from nanohole arrays, nanoslit arrays have two different natures of resonances: the surface plasmon resonance on the outside gold/air interface (SPR mode) (Collin et al., 2001; Moreau et al., 2007) and gap plasmon resonance in the nanoslits (cavity mode) (Takakura, 2001; Cao and Lalanne, 2002). Both resonances cause enhanced light transmission. Previous studies focused on the SPR mode and its biosensing capability. To our knowledge, there are no studies related to the surface sensitivity of the gap plasmons. In this paper, we first verified the gap plasmon's sensitivity in nanoslit arrays with various slit widths. By coating different kinds of biomolecules on the nanoslit surface, we confirmed that resonant peak caused by gap plasmons has a larger redshift than that of the SPR mode. There is little correlation between the slit width and the sensitivity of SPR mode. However, the sensitivity of cavity mode is substantially increased with the decrease of slit width. Its sensitivity is increased 10 times when the slit width is reduced to 30 nm.

2. Fabrication of metallic nanoslits

Gold nanoslit arrays were fabricated by using electron-beam lithography and a reactive-ion etching machine. We used a glass

* Corresponding author at: Research Center for Applied Sciences, Academia Sinica, No. 128, Section 2, Academic Road, Taipei, 11529, Taiwan. Tel.: +886 2 27898000; fax: +886 2 26826680.
E-mail address: pkwei@gate.sinica.edu.tw (P.-K. Wei).

0956-5663/$ – see front matter © 2008 Elsevier B.V. All rights reserved.
doi:10.1016/j.bios.2008.03.044

slide as the substrate. Gold has poor adhesion to the glass surface, hence a 5 nm-thick Ti film was deposited before a 130 nm-thick gold film by using an electron gun evaporator. After the deposition, a 350 nm-thick PMMA resist (MicroChem) was spin-coated on the sample. A field-emission scanning electron microscope modified with a nano-pattern generating system (NPGS) was used to write nanoslits on the PMMA resist. The patterns were then transferred to Ti/Au film by using argon sputtering in a reactive-ion etching machine (Oxford Instrument). The power of the radiofrequency wave in the reaction chamber was 200 W. The flow rate of Ar gas was 40 sccm. The PMMA resist was then removed by rinsing the sample in acetone for a few hours. To make sure that no PMMA residue remained in the gold nanoslits, we further cleaned the sample by using ozone sputtering. The sample was put in ultrapure water and placed in an ultrasound bath for 20 min. After the ultrasonic cleaning, the sample was purged dry by nitrogen.

In our experiments, we fabricated gold nanoslit arrays with different periods and slit widths. The "period" is the distance to repeat a nanoslit. When we changed the period, we increased the space between two slits. Fig. 1(a) shows a SEM image for periodic gold nanoslits on a glass substrate. The period was 600 nm and slit width was about 80 nm. Fig. 1(b) shows transmission optical images of different nanoslit arrays. These images were taken by a 4× objective and a color CCD. The slit width varied from 20 nm to 100 nm. Area of each nanoslit array was 150 μm × 150 μm. The colors of nanoslit arrays are due to extraordinary transmission of the surface plasmon resonance. It is noted that these colors are not only

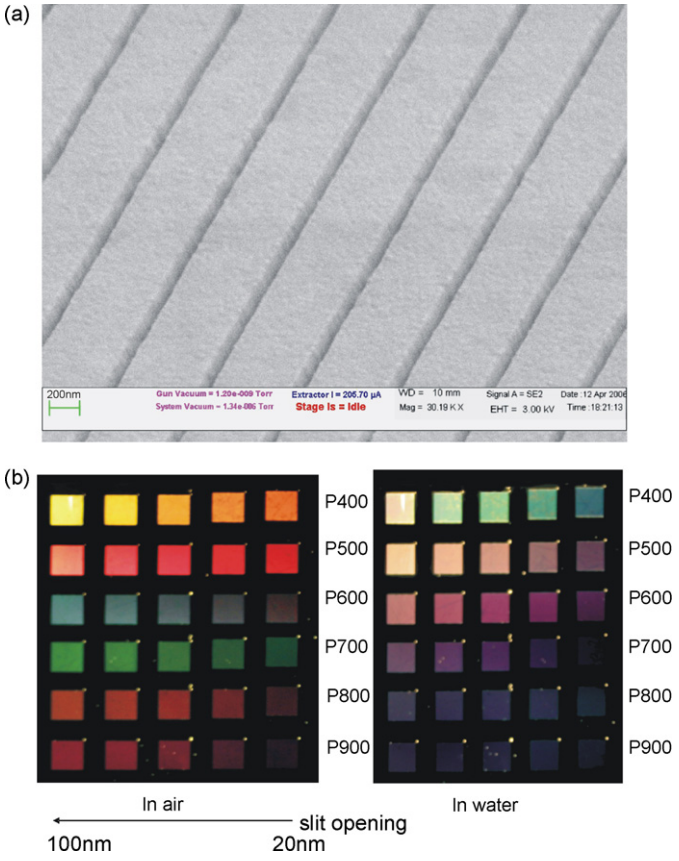

Fig. 1. (a) The SEM image of a gold nanoslit array. The array had a period of 600 nm and the slit width was about 80 nm. (b) The transmission optical Images of various nanoslit arrays in air and in water environment. The array period changed from 400 nm to 900 nm and slit width, from 20 nm to 100 nm. The area of each nanoslit array was 150 μm × 150 μm. The colors of the nanoslit arrays are due to extraordinary transmissions of surface plasmon resonances.

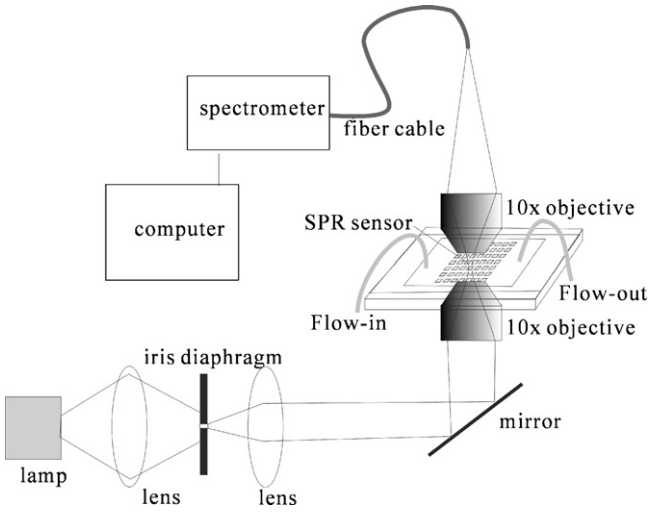

Fig. 2. The optical setup for transmission spectrum measurement. The light source is a 12 W halogen lamp. The iris diaphragm and 10× objective lens made an optical spot smaller than 150 μm in diameter on the sample surface. The transmission light is delivered by a fiber cable and measured by a linear CCD array spectrometer.

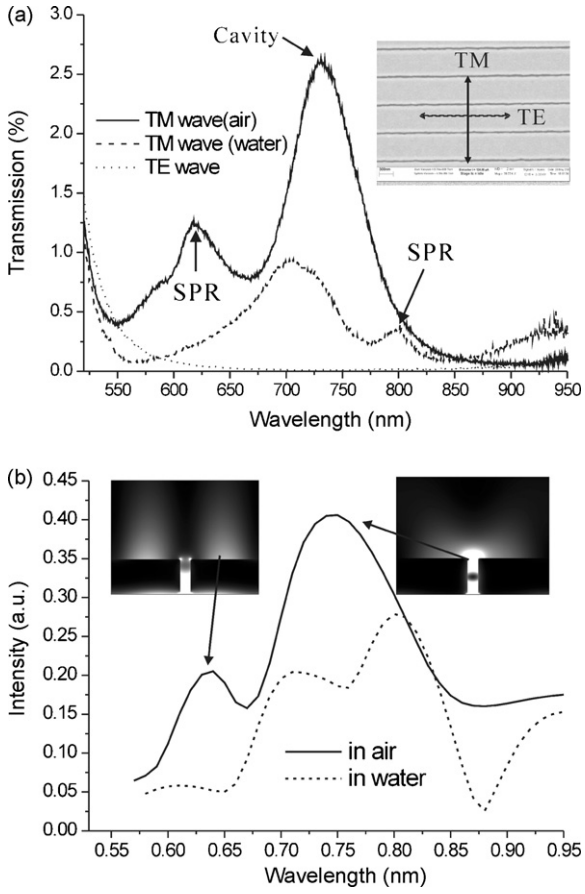

Fig. 3. (a) The measured transmission spectra of a 600 nm-period, 80 nm-slit width gold nanoslit array with different incident polarizations. For TE polarized wave, the transmission intensity is decreased with wavelength. For TM wave, there are two enhanced transmission peaks. The 735 nm peak is due to the cavity mode. The 624 nm is attributed to SPR mode at the outside air/gold interface. The 800 nm wavelength is a SPR mode in water. (b) The calculated transmission spectrum of a 600 nm-period nanoslit array in air and in water. The insets show optical field distributions for both SPR mode and cavity mode in air.

changed with the period but also affected by the slit width and surface environment.

3. Measurement results and discussion

Transmission spectra for gold nanoslit arrays were measured by using a 12 W halogen lamp. Fig. 2 shows the optical setup. The light was spatially filtered by using an iris diaphragm and a collimation lens. Its incident polarization was controlled by a linear polarizer. The polarized light was then focused on a single array by using a 10× objective lens. To avoid influence of other arrays, the beam size focused on the array needs to be smaller than 150 μm. This was accomplished by adjusting the aperture size of the diaphragm. The transmission light was then collected by another 10× objective lens and focused on a fiber cable. The transmission spectrum was measured by using a fiber-coupled linear CCD array spectrometer (BWTEK).

Fig. 3(a) shows the measured transmission spectra of a 600 nm-period nanoslit array. The transverse-electric (TE) polarized light cannot generate surface plasmon in the nanoslit structures. The optical transmission shows exponentially intensity decay with the wavelength. On the other hand, the surface plasmons can be excited by using transverse-magnetic (TM) wave. There were two apparent resonant peaks at wavelengths of 624 nm and 735 nm. The 624 nm peak wavelength is due to horizontal resonances of surface plasmons at the outside air/gold interface. This SPR wavelength can be predicted by the phase matching condition, $\lambda_{SPR} = \sqrt{[\varepsilon_m \varepsilon_s/(\varepsilon_m + \varepsilon_s)]}P$, where P is the period and ε_m and ε_s are the permittivities of metal and surface medium. In this calculation, the permittivity of gold should be changed with the wavelength. The ε_m vs. the wavelength can be found elsewhere (Palik, 1991). In air, the calculated SPR wavelength is 626.68 nm (P = 600 nm, ε_s = 1, $\varepsilon_m \sim -12$) agreed quite well with the measured one. In water, the SPR wavelength shifts to 809 nm (P = 600 nm, $\varepsilon_s = 1.3^2$, $\varepsilon_m \sim -24$). This peak can be found when the sample was covered with water. The 735 nm peak is due to the resonance of gap plasmons in the slit. The gap plasmon is known to be a non cut-off TM wave propagating in the nanometer slit gap (Wei et al., 2002).

The SPR mode and cavity mode are further verified by the theoretical calculations. Fig. 3(b) shows the calculation results by using finite-difference time-domain (FDTD) method (Taflove and Hagness, 2000). In air, there are two transmission peaks. The positions of peak wavelengths are consistent with the measured values. In water, the calculation result shows two transmission peaks sim-

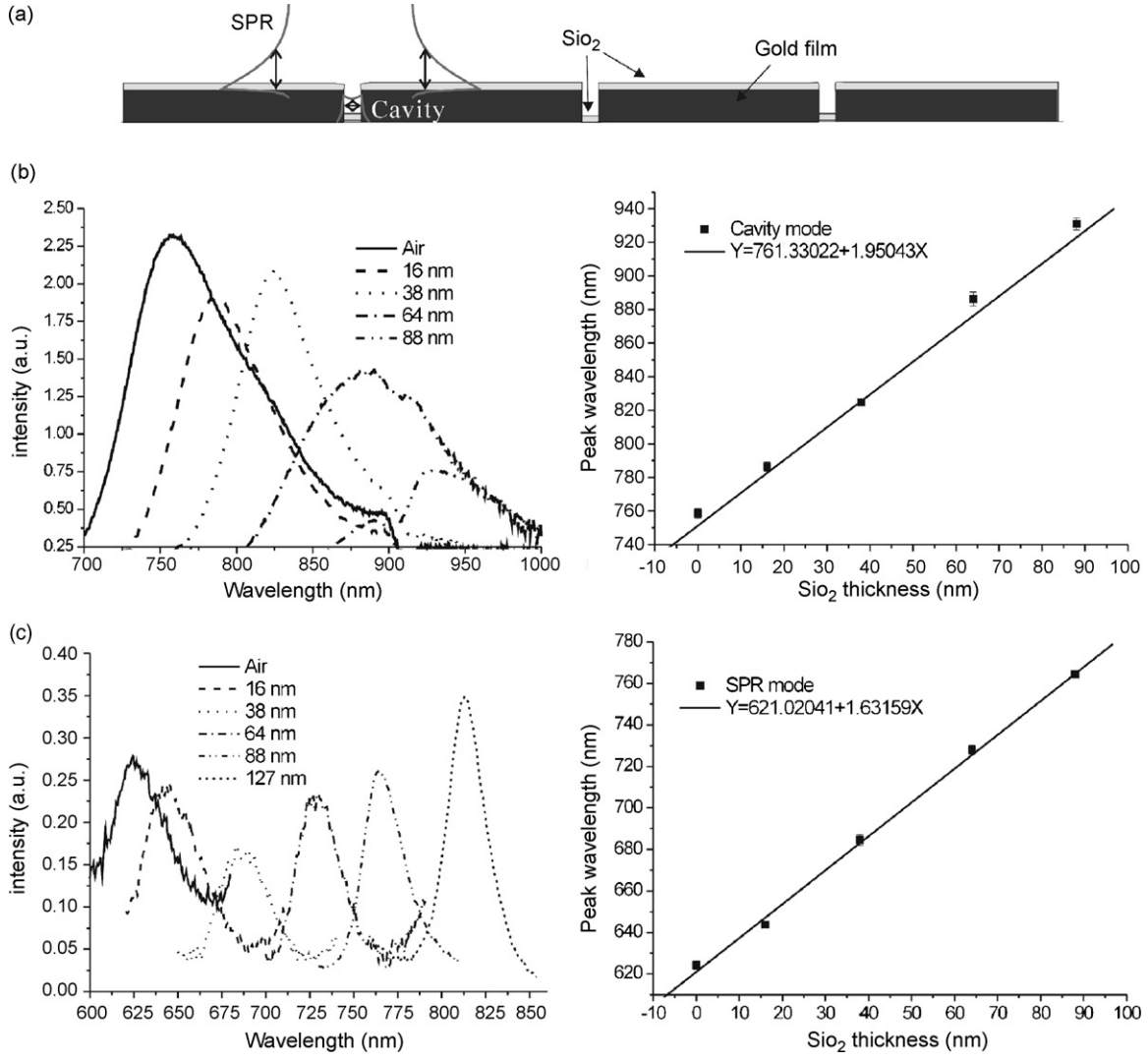

Fig. 4. (a) The distribution of SiO_2 film on a nanoslit array. (b) The measured transmission spectra of a 600 nm-period nanoslit array with various thicknesses of SiO_2 films. Left: the transmission spectra of the cavity mode. Right: the peak wavelength vs. the SiO_2 thickness. (c) Left: the transmission spectra of the SPR mode. Right: the peak wavelength vs. the SiO_2 thickness.

ilar to the measured ones, except that the relative peak value is different. We plot optical field distribution at different peak wavelength in air. At 630 nm peak, the optical wave is localized on the outside surface. The optical distribution is due to the interference of surface plasmons propagating along opposite directions. At 735 nm peak, the slit gap has a strong localized optical field. Due to the resonance of gap plasmon, there is a node at the middle of the slit height.

The experiments and theoretical calculations verify two distinguishable plasmon resonances in a 600 nm-period array. Therefore, we used the nanoslit array to compare the detection sensitivities. Fig. 4 shows the measured transmission spectra with various thicknesses of SiO_2 film. Fig. 4(a) illustrates the deposition of SiO_2. In the experiment, the SiO_2 films were deposited on the nanoslit array by using a thermal evaporator. The sample was placed above the SiO_2 source without inclination. As a result, SiO_2 thin film was grown from the bottom. The film thickness varied from 16 nm to 127 nm. The black line was the transmission spectrum of the nanoslit array in air. When SiO_2 film was deposited on the nanoslit surface, there was significant change in the peak wavelengths and transmission intensity.

For the cavity mode (Fig. 4(b)), the resonant wavelength has a redshift and is linearly increased with the increase of SiO_2. A classic Fabry–Perot model can illustrate the cavity resonance. In the nanoslit, the optical wave is in resonance when its phase satisfies

$$\frac{4\pi nh}{\lambda_0} + \phi_1 + \phi_2 = 2m\pi \quad (1)$$

where n is the equivalent refractive index in the slit, λ_0 is the free space wavelength, h is the thickness of gold film, m is the mode number, and ϕ_1 and ϕ_2 are the phase shifts at the top and bottom interfaces. A nanometer-scale increase of SiO_2 results in a little increase in equivalent refractive index. Hence, the resonant wavelength is linearly increased with the thickness as shown in Fig. 4(b). It is noted when the nanoslit array is filled with water, the refractive index is substantially changed from 1 to 1.33. As a result, the fundamental cavity mode is moved to the infrared (IR) region. In Fig. 3(a), the 800 nm-wavelength is the SPR mode in water. There is another peak at ~700 nm wavelength. This peak comes from high order cavity mode, not the blueshift of the fundamental mode. The fundamental mode has the highest sensitivity. However, its peak in water moves to the IR region. It is necessary to have a bright IR source and a sensitive, high-resolution IR spectrometer to study bio- or chemical reactions in water environment.

For the SPR mode (Fig. 4(c)), the 624 nm peak was also red shifted to meet phase matching condition, yet its transmission intensity increased for thick SiO_2 film. This enhanced transmission is attributed to the increased SPR coupling between top surface and bottom surface of the gold film. Minimizing the difference between the SPR modes on both surfaces increases the transmission efficiency. A strong resonance occurs when the difference is zero (Krishnan et al., 2001). The sensitivities of cavity mode and SPR mode can be compared by plotting peak wavelengths as a function of the SiO_2 thickness. The slopes of the fitting curves show that the sensitivities were 1.95 and 1.63 for the cavity mode and the SPR mode, respectively. It indicates the wavelength sensitivity of cavity mode was about 1.2 times larger than that of SPR mode. With this sensitivity, the cavity mode can detect a 0.05 nm-thick SiO_2 film attached to the surface if the resolution of a spectrometer is 0.1 nm.

The SPR mode is determined by the phase matching condition. It implies that SPR mode is independent with the slit width. To increase the SPR sensitivity, a simple way is to increase the period (Pang et al., 2007). On the other hand, the cavity mode is formed by gap plasmon resonance. Its detection sensitivity is dependent to the height and width of the nanoslits. To study the cavity mode sensitivity as a function of the slit width, we coated small biomolecules on various nanoslit arrays. The small molecule was galactose, a type of 180.08 Da sugar. With chemical modification, galactose with a sulfhydryl group (282.32 Da) can be adsorbed on gold surface. In the experiment, the transmission spectrum of the nanoslit array in air was first taken. Then 0.01 mg/μl galactose solution was dropped on the gold surface. The sample was placed for 3 h in order to attach the modified galactose to the gold surface. The sample was then purged dry by nitrogen and measured again. Fig. 5(a) shows the transmission spectra of various nanoslit arrays with and without the modified galactose. When galactose attached to the array, there was a redshift in the peak wavelength and a significant decrease of transmission intensity in the cavity mode. The change was not found for the SPR mode.

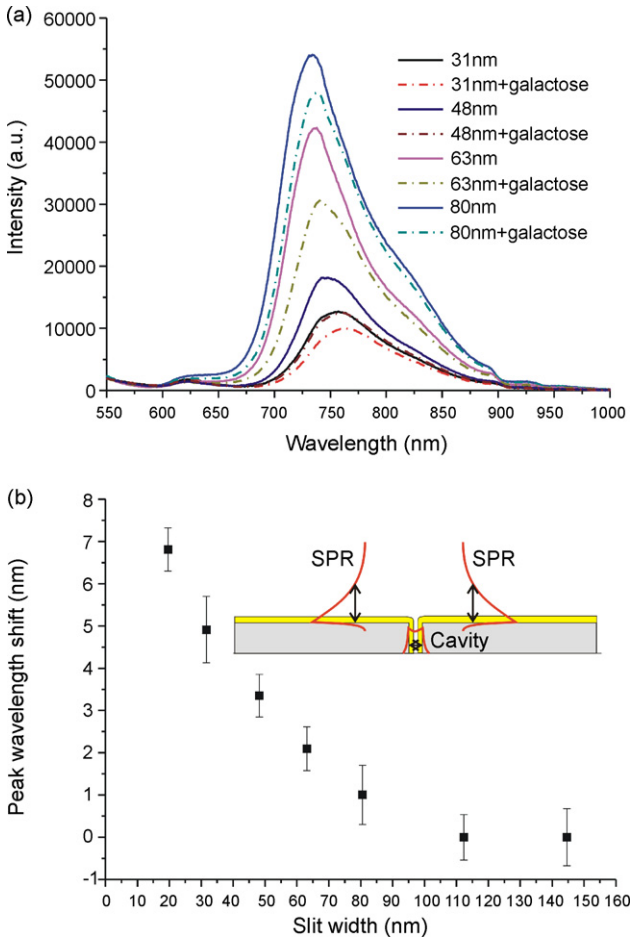

Fig. 5. (a) The transmission spectra of various nanoslit arrays with and without the modified galactose on the gold surface. The slit widths were 31 nm, 48 nm, 63 nm and 80 nm, respectively. (b) The peak wavelength shift vs. the slit width for the cavity mode. The shift was increased when the slit width was decreased from 100 nm to 20 nm. The inset shows the schematic of the optical field distributions for SPR mode and cavity mode. The width of the cavity mode is decided by the slit width. The overlap between biomolecules and the cavity mode is large for very narrow slits.

Fig. 5(b) shows the peak wavelength shift vs. the slit width for the cavity mode. The shift was the difference of transmission peaks with and without the galactose. The shift increased when the slit width was reduced from 100 nm to 20 nm. The peak wavelength shifted about 6.80 nm, 3.35 nm and 1.00 nm for 20 nm, 50 nm and 80 nm-wide nanoslits, respectively. These values imply that if the resolution of a spectrometer is 0.1 nm, the nanoslit can detect ~4 Da, 8 Da, and 28 Da-sized biomolecules, respectively. The modified galactose was not detectable when the slit width was

larger than 90 nm. The cavity mode sensitivity is dependent on the slit width and can be improved by narrowing the slits. We attribute the sensitivity enhancement to the large overlap between the biomolecules and the plasmonic mode profile. The inset in Fig. 5(b) shows the schematic of optical distributions of the SPR mode and the cavity mode. The SPR mode has an evanescent tail perpendicular to the surface. The length of the evanescent tail can be estimated by the equation, $\lambda_0/2\pi\sqrt{n_{\text{eff}}^2 - 1}$, where n_{eff} is the equivalent refractive index of the SPR mode. The length is about 150 nm at a wavelength of 630 nm. This length is independent with the slit width. On the hand, the cavity mode is confined in the gap. Its width is controlled by slit opening. The overlap between the biomolecules and the cavity mode becomes large when the slit width is very small.

The galactose is too small to identify the changes in SPR modes. Therefore, we compared surface sensitivities of both modes by using the protein–protein interactions. We applied 600 nm-period nanoslit arrays to detect the bovine serum albumin (BSA, 66kDa size) and anti-BSA on gold surface. The buffer solution, 10 mM phosphate-buffered saline (PBS), was dropped on the sample. After drying the sample, we took the transmission spectrum of the nanoslit array. Then 1 mg/ml BSA was put on the nanoslit surface. The sample was placed for 3 h in order to attach BSA to the gold surface. The PBS buffer washed the sample twice to remove the unbound proteins. The spectrum of the nanoslit array was taken. Finally, 0.47 mg/ml anti-BSA was put on the nanoslit surface. After 3-h protein–protein interactions, the unbound anti-BSA was washed away by the PBS buffer. The transmission spectrum was then taken.

Fig. 6(a) shows the normalized transmission spectra of the nanoslit array. The slit width of the array was ~60 nm. It is clear that redshift of cavity mode is much larger than that of the SPR mode. For the SPR mode, the BSA proteins resulted in a 6.32 nm redshift. The shift was further increased to 9.06 nm when anti-BSA was bound to BSA. For the cavity mode, BSA proteins resulted in a 15.2 nm redshift. It increased to 22.9 nm when anti-BSA was bound to the BSA. In the ~60 nm-wide slit, the cavity mode is about 2.5 times sensitive than that of the SPR mode. The SPR mode sensitivity of gold nanoarrays have been measured and confirmed by different groups (Brolo et al., 2004; Pang et al., 2007; Lee et al., 2007). Its sensitivity is similar to the conventional grating-based SPR sensor. In the experiments, we used high concentration BSA and un-modified gold surface to make sure that the condition is the same for both SPR mode and cavity mode. The 1 mg/ml BSA concentration is not aimed for testing detection limits. For such test, surface modification of gold film is necessary to increase the immobilization of BSA.

To show that the cavity mode sensitivity is slit width dependent, we further compare the wavelength shifts in various nanoslit arrays with and without the BSA coating. Fig. 6(b) shows the peak wavelength shift vs. the slit width for the cavity mode and SPR mode. The surface sensitivity of SPR mode was not significantly improved when the slit width was decreased. Nevertheless, the cavity mode became very sensitive when the slit width was smaller than 50 nm. The cavity mode and SPR mode had a similar sensitivity when slit width was ~80 nm. When slit width was reduced to 30 nm, the cavity mode had a sensitivity one order of magnitude larger than that of the SPR mode. It is noted there is a large sensitivity variation in the cavity mode. It is due to the fabrication inaccuracy of the nanoslit arrays. In the experiment, the nanoslit arrays were designed by the NPGS software and made by an electron-beam writer and a reactive-ion etching machine. The fabrication resolution of our machines was about 5 nm. Therefore, for several 10 nm wide slits, there exist fabrication variations. The gap plasmon is sensitive to the slit width, hence its sensitivity in Fig. 6(b) appears variable.

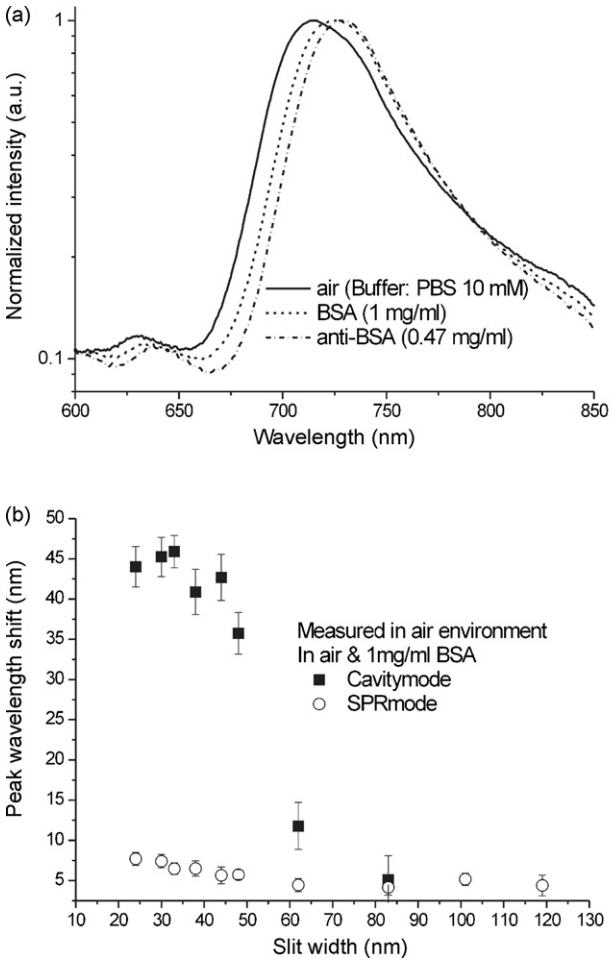

Fig. 6. (a) Normalized transmission spectra of BSA and anti-BSA interactions on a 600 nm-period and 60 nm-slit width nanoslit array. The wavelength shift of the cavity mode is larger than that of the SPR mode. (b) The peak wavelength shift vs. the slit width for the cavity mode and SPR mode. The biomolecules were 66 kDa-sized BSA. The detection sensitivity of SPR mode was not significantly improved when the slit width was changed. Nevertheless, the cavity mode becomes very sensitive when slit width is smaller than 50 nm.

4. Conclusions

We studied the surface sensitivity of gap plasmon resonance in gold nanoslit arrays and compared it with conventional SPR sensors. The BSA and anti-BSA interactions verified the surface sensitivity of cavity mode is much better than the SPR mode. The result of galactose coating indicates the cavity mode has a detection limit of ~4 Da-sized biomolecules when wavelength resolution is 0.1 nm. The sensitivity of the cavity mode is found dependent on the slit width. It increased 10 times when the slit width was reduced from 100 nm to 30 nm. The high sensitivity of cavity mode is attributed to the large overlap between the biomolecules and nanometer gap plasmons. Gap plasmons based biosensors are easily applied for two dimensional, high-throughput detections. There are several two dimensional SPR devices. For example, the prism-based device can take two dimensional SPR images by using the changes in optical phase associated with the SPR condition. However, its dynamic range is small because the phase changes are periodic. In our nanoslit array, the gap plasmon sensor has a larger dynamic range and better linear response as seen in Fig. 4(a). The high-throughput SPR device can also be achieved by using two dimensional grating arrays. The device has to be operated in the refection mode with precise control

of incident angle. The gap plasmon in the nanoslit array has a higher sensitivity than the grating-based device. In addition, its spectrum is taken in the transmission mode with normal incidence. The transmission light is dominated by the localized surface plasmons. The incident angle has little effect on excitation of plasmons. The disadvantage of the nanoslit device is the fabrication cost. We currently use electron-beam lithography to prepare the nanoslit array. Since the structure of the nanoslit array is simple and periodic, advanced nanotechnologies such as nanoimprinting could be used for the mass fabrication to reduce the cost.

Acknowledgements

The authors would like to thank Professor Chun-Cheng Lin and Ms. Shu-Yi Hsieh, Ph.D. candidate, of National Tsing Hua University for providing the modified galactose and Dr. Shih-Hsin Hsu of Research Center for Applied Sciences, Academia Sinica, for facility support. This research is supported by the National Science Council, Taiwan (Grant No. NSC 95-2215-E-001-001) and the Thematic Project of Academia Sinica, Taiwan.

References

Brolo, A.G., Gordon, R., Leathem, B., Kavanagh, K.L., 2004. Langmuir 20, 4813–4815.
Cao, Q., Lalanne, P., 2002. Phys. Rev. Lett. 88, 057403.
Collin, S., Pardo, F., Teissier, R., Pelouard, J.L., 2001. Phys. Rev. B 63, 033107.
Ebbesen, T.W., Lezec, H.J., Ghaemi, H.F., Thio, T., Wolff, P.A., 1998. Nature 391, 667–669.
Gavin, M.B., Stuart, L.S., 2000. Science 289, 1760–1763.
Homola, J., Yee, S.S., Gauglitz, G., 1999. Sens. Actuators B54, 3–15.
Kawata, S., 2001. Near-Field Optics and Surface Plasmon Polaritons, first ed. Springer, New York.
Knoll, W., 1998. Annu. Rev. Phys. Chem. 49, 569–639.
Krishnan, A., Thio, T., Kim, T.J., Lezec, H.J., Ebbesen, T.W., Wolff, P.A., Pendry, J., Martin-Moreno, L., Garcia-Vidal, F.J., 2001. Optics Commun. 200, 1–7.
Lee, K.L., Lee, C.W., Wang, W.S., Wei, P.K., 2007. J. Biomed. Opt. 12 (4), 044023.
Lezec, H.J., Degiron, A., Devaux, E., Linke, R.A., Martin-Moreno, L., Garcia-Vidal, F.J., Ebbesen, T.W., 2002. Science 297, 820–822.
Moreau, A., Lafarge, C., Laurent, N., Edee, K., Granet, G., 2007. J. Opt. A: Pure Appl. Opt. 9, 165–169.
Palik, E.D., 1991. Handbook of Optical Constants of Solids, II. Academic, New York.
Pang, L., Hwang, G.M., Slutsky, B., Fainman, Y., 2007. Appl. Phys. Lett. 91, 123112.
Schena, M., Shalon, D., Davis, R.W., Brown, P.O., 1995. Science 270, 467–470.
Silin, V., Plant, A., 1997. Trends Biotechnol. 15, 353–359.
Taflove, A., Hagness, S.C., 2000. Computational Electrodynamics: The Finite-Difference Time-Domain Method, second ed. Artech House, Boston.
Takakura, Y., 2001. Phys. Rev. Lett. 86, 5601–5603.
Wei, P.K., Chou, H.L., Fann, W.S., 2002. Opt. Express 10, 1418–1424.